



**Size-Controlled Synthesis of Mesoporous Palladium Nanoparticles as Highly Active and Stable Electrocatalysts**

Journal:	<i>ChemComm</i>
Manuscript ID:	CC-COM-06-2014-004955.R1
Article Type:	Communication
Date Submitted by the Author:	26-Jul-2014
Complete List of Authors:	Cuiling, Li; National Institute for Materials Science, WPI Center for MANA Sato, Takaaki; Shinshu University, Yamauchi, Yusuke; National Institute for Materials Science, WPI Center for MANA

Cite this: DOI: 10.1039/c0xx00000x

www.rsc.org/xxxxxx

## COMMUNICATION

## Size-Controlled Synthesis of Mesoporous Palladium Nanoparticles as Highly Active and Stable Electrocatalysts

Cuiling Li,<sup>a</sup> Takaaki Sato<sup>b</sup> and Yusuke Yamauchi<sup>\*a,c</sup>

Received (in XXX, XXX) Xth XXXXXXXXX 20XX, Accepted Xth XXXXXXXXX 20XX

DOI: 10.1039/b000000x

We report a solution phase synthesis of monodispersed mesoporous Pd nanoparticles (MPNs) with narrow particle size distributions. The average particle sizes can be controlled to a range of 25 nm to 42 nm, by utilizing cationic surfactants (as a structure-direct agent) and triblock copolymers (as a protective agent for controlled Pd deposition). The obtained MPNs exhibit very high electrocatalytic activity in formic acid oxidation.

Various porous architectures have been prepared using molecular templates; in particular, self-assembly of amphiphilic molecules has attracted much attention in mesoporous materials design. Significant research efforts have been devoted to the development of various types of mesoporous materials such as nanoparticles, fibers, films, and bulks.<sup>[1]</sup> Currently, mesoporous nanoparticles (MNs), the size of which is less than 50 nm, have drawn increasing attention because of the general characteristics of porous materials and the effective utilization of pores in nanosized particles.<sup>[2]</sup> Controlling the particle size, uniformity, and dispersity of MNs has been extensively studied with an eye toward target applications. However, the compositions reported previously are mainly silica and carbon based, which have been used in catalysts, adsorbents, fillers, optical devices, and biomedical applications.

In particular, MNs with metallic frameworks attract considerable interest because of their beneficial uses as superior metal catalysts. Hard templates, which have been employed for synthesis of mesoporous metal oxides and carbons<sup>[3a-b]</sup>, can be utilized for preparation of mesoporous metals.<sup>[3c-g]</sup> This hard-templating method needs several steps (*i.e.*, preparation of mesoporous matrix, deposition of inorganic compositions inside the mesopores, and removal of the mesoporous matrix). Soft templates composed of self-assembled micelle structures (*e.g.*, lyotropic liquid crystals<sup>[4a-b]</sup>) have been also used for producing mesoporous metals.<sup>[4c-d]</sup> Mesoporous Pt-based materials have been synthesized by chemical or electrochemical deposition methods. In spite of recent significant advancements in soft- and hard-templating methods, they are mainly limited to producing simple morphologies (*e.g.*, irregularly shaped particles and films) because of the inflexibility and limitations of both common methods.

In this paper, we demonstrate the first successful synthesis of uniformly sized mesoporous Pd nanoparticles (MPNs) with periodically ordered mesostructures. Currently, nanostructured

palladium (Pd) has attracted considerable interest among researchers due to its important role in several catalytic reactions.<sup>[5]</sup> However, well-defined MPNs whose particle sizes are less than 50 nm have not been realized yet, because it is difficult to precisely control Pd deposition behavior on molecular templates. Wang *et al.* nicely reported porous single-crystalline Pd nanoparticles in a wide range of particle sizes from 14 nm to 53 nm, but unfortunately they failed to realize the high surface area by gas adsorption measurements owing to the aggregation and coalescence caused by drying.<sup>[5b]</sup> Our MPNs with well-developed mesoporous structures exhibit high surface areas which allow an abundant supply of active sites to promote high accessibility of guest molecules from the outside. Here, we realized the formation of MPNs by utilizing cationic surfactants (as a structure-direct agent) and triblock copolymers (as a protective agent for controlled Pd deposition).

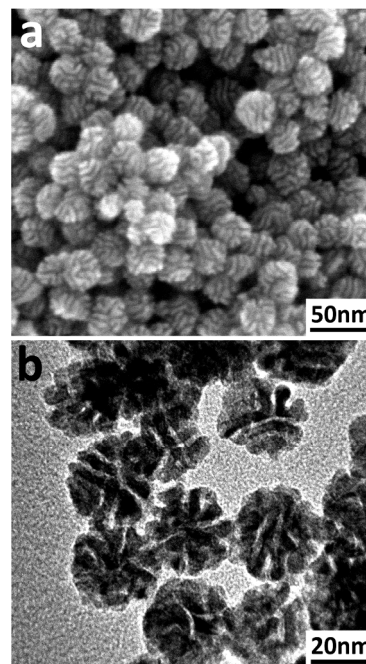


Fig. 1 SEM and TEM images of MPNs prepared under typical condition (1.0wt% F127).

In a typical synthesis of MPNs, a cationic hexadecylpyridinium chloride (HDPC) surfactant was thoroughly dissolved in deionized water to obtain a transparent solution.

After that, nonionic block triblock polymer (Pluronic F127) solution was mixed (In this typical condition, the concentration of F127 is 1.00 wt%). Then, sodium tetrachloropalladate ( $\text{Na}_2\text{PdCl}_4$ ) solution was added as a Pd source. After the addition of ascorbic acid solution as a reducing agent, the reaction solution was incubated. The resulting colloidal products were collected by centrifugation and washed several times using ethanol and water. The details are given in the supporting information. Mixed surfactants/polymers systems have been known for preparation of mesoporous silica nanoparticles<sup>[6]</sup>, but never been utilized for controlling metal deposition behavior. This is the first report of fine tuning of particle sizes of MPNs.

The representative electron microscopic images of MPNs prepared under typical conditions are shown in Fig. 1. The images clearly show that all the particles possess a highly porous structure, and the connected porous channels together with the Pd frameworks create a walnut-like shape. Any byproducts, such as non-porous particles and bulks, were not observed, demonstrating high-yield synthesis of the MPNs. Under typical conditions, the particle sizes ranged narrowly from 25 to 35 nm, with an average diameter of approximately 28 nm (Fig. S1d). In highly magnified SEM and TEM images (Figs. 1 and S2), it was clearly observed that tubular structures that were bent in a random manner were formed inside the particles. To evaluate the presence of porosity,  $\text{N}_2$  gas adsorption isotherms were measured. Owing to such high porosity, the BET surface area was calculated to be  $51.4 \text{ m}^2\cdot\text{g}^{-1}$  (Fig. S3). Uptake of nitrogen gas at relative pressure range of 0.8-0.95 is attributed to the formation of interparticle space. To measure the electrochemically active surface area (ECSA) of our MPNs, cyclic voltammetry (CV) measurement was conducted in  $0.5 \text{ M H}_2\text{SO}_4$  solution with a scan rate of  $50 \text{ mV}\cdot\text{s}^{-1}$  (Fig. S4). By considering the charge required for desorption of a monolayer of hydrogen on Pd surface ( $210 \mu\text{C}\cdot\text{cm}^{-2}$ ), the ECSA of MPNs was calculated to be  $61.8 \text{ m}^2\cdot\text{g}^{-1}$  which was around 30 % increase compared to commercially available Pd (PB) ( $47.8 \text{ m}^2\cdot\text{g}^{-1}$ ). Thus, the high surface area of our MPNs was confirmed by both the gas adsorption and the electrochemical analysis.

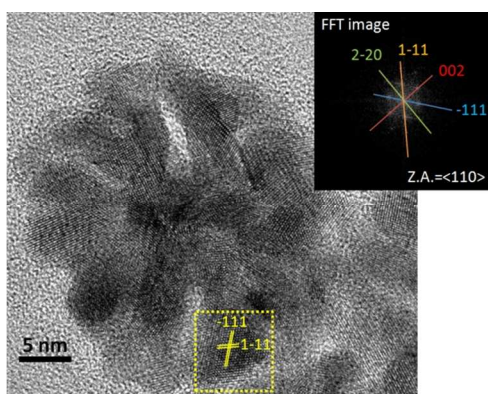


Fig. 2 Highly magnified TEM image of MPNs prepared under typical condition (1.0 wt% F127) and FFT image taken from the yellow-colored square area.

The crystallinity of MPNs was further investigated using high-resolution TEM (HRTEM) (Fig. 2) and electron diffraction (ED) (Fig. S5). From the HRTEM image of a whole particle, it was proved that the frameworks were highly crystallized without any amorphous phase (Fig. 2). The ED patterns taken from one

individual particle show intense spots assignable to face-centered-cubic (*fcc*) structure (Fig. S5). Appearance of additional weak spots indicates that different crystal domains exist as minor phases. Therefore, individual particles are not perfect single crystals, but the pore walls are highly crystallized and the lattice fringes are oriented in the same direction in some parts. As shown in Fig. S6, however, it should be noted that the crystal fringes were randomly oriented in the center part of MPN. The wide-angle X-ray diffraction (XRD) profile is assigned to a Pd *fcc* crystal without any impurity phases (Fig. S7).

The electronic states of the obtained MPNs were also investigated by X-ray photoelectron spectroscopy (XPS) (Fig. S8). Two main peaks at binding energy of 335.2 and 340.4 eV correspond to the  $3d_{5/2}$  and  $3d_{3/2}$  spin orbit, respectively, splitting from the Pd 3d cores (Fig. S8a). From the fitting data, four component peaks were clearly observed. A portion of the Pd surface was slightly oxidized, but the main contribution was  $\text{Pd}^0$ , which is consistent with an assignment of the metallic Pd. No signal from the N 1s region indicates that the surfactants are completely removed from the MPNs using the present washing procedure (Fig. S8b).<sup>[7]</sup>

To understand the formation mechanism of MPNs, we prepared MPNs without F127. The obtained MPNs were irregularly shaped, and their particle sizes were relatively large, above 40 nm (Figs. S1a and S9). Regardless of the absence of nonionic F127, a similar mesostructure was formed in the particles (Fig. S9). The distance between the neighboring tubular structures was constant (around 2.5 nm). As another experimental, the Pd species were reduced in the absence of both F127 and HDPC surfactants, in which the deposited Pd particles had no porous structures (Fig. S10). From these results, it proved that only cationic HDPC plays a critical role in the formation of mesostructures inside the particles. In the reaction solution, the positively charged  $\text{HDP}^+$  species effectively interacted with the  $[\text{PdCl}_4]^{2-}$  species dissolved in solution, as clearly confirmed by UV-Vis absorption spectra (Fig. S11b). After the addition of HDPC, the spectrum of  $\text{Na}_2\text{PdCl}_4$  solution was significantly changed, and a newly formed absorption peak was observed at 290 nm (The change of solution colors is also shown in Fig. S11a). This is caused by the strong interaction between the positively charged  $\text{HDP}^+$  and the  $[\text{PdCl}_4]^{2-}$  species.<sup>[8]</sup> Actually, this absorption peak gradually increased by increasing the amount of  $\text{Na}_2\text{PdCl}_4$  used in the solution (Fig. S11c). Furthermore, we prepared several MPNs by changing the amount of F127 (Figs. S1 and S12). It is important to note that the coexistence of F127 significantly affected the particle sizes. As shown in Fig. S1, by increasing the amount of F127 (from 0.00 wt% to 0.25 wt%, 0.5 wt%, 1.0 wt%, and 1.5 wt%), the particle sizes gradually decreased from 42 nm to 34 nm, 31 nm, 28 nm, and 25 nm, without any difference in the mesostructural ordering (Figs. S1 and S12). The above concept is also applicable to other cationic surfactants, such as hexadecyltrimethylammonium chloride (CTAC). We replaced HDPC with CTAC for preparation of MPNs (Fig. S13). Similar as HDPC system, the average particle sizes were gradually decreased with the increase of the amount of F127 (Fig. S14), although the mesostructural ordering formed inside the MPNs was not so high (Fig. S13).

On the basis of the above results, the present reaction model is

supposed as follows. As the used HDPC concentration is above the critical micelle concentration (CMC, 0.9 mM), the micelles really exist in the solution. At the early stage of reaction, small Pd clusters (*i.e.*, nuclei) are generated, and grain growth starts from these initial nuclei. During the Pd deposition, the Pd species approach the nuclei along with the cationic surfactants. Therefore, the local concentration of the surfactants on the particle's surface is considered to be higher than that in a bulk solution.<sup>[9]</sup> At this stage, a structural change in the micelles from spheres to tubular structures would take place thermodynamically to minimize the total energy of the system. Cationic surfactants with the same alkyl chains (C<sub>16</sub>) have often been utilized for the preparation of mesoporous silica materials with pore sizes of 2.1–2.6 nm<sup>[10]</sup> These values are close to the pore size observed in **Fig. 1a**, suggesting that HDPC serves as a structure-direct agent. The nonionic triblock copolymer was able to surround the deposited Pd/HDP composites of a certain size due to a weak interaction between the ionic and nonionic hydrophilic groups. Thus, the presence of F127 micelles covering the nanoparticles suppressed the grain growth and stabilized the ordered mesostructures.

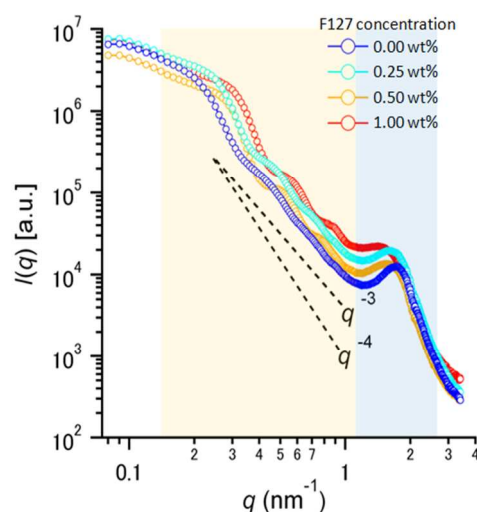


**Fig. 3** SAXS intensities  $I(q)$  of MPNs particles prepared with varied F127 concentration as a function of the magnitude of the scattering vector  $q$ . Orange-colored region highlight the interference peaks arising from the positional correlations between the particles, while blue-colored region indicates the reflection from the periodicity of mesostructures.

**Fig. 3** shows SAXS intensities  $I(q)$  of the obtained MPNs prepared with varied F127 concentrations, where  $q$  is the magnitude of the scattering vector. We observed the appearance of the interference peak in a low  $q$  range (the orange-colored region), which arises from positional correlations between HDPC particles. Increasing the F127 concentration leads to a pronounced high- $q$  shift of the peak position, meaning a gradual decrease of the average particle sizes (as shown in **Fig. S1**). A fractal or “rough” surface of the particles shows up directly in the slope of a log-log plot [ $I(q)$  vs.  $q$ ] in the Porod regime as  $I(q) \propto q^{-(6-D_s)}$ , where  $D_s$  denotes the surface fractal dimension.<sup>[11]</sup> A smooth surface ( $D_s = 2$ ) gives  $q^{-4}$  the behavior of  $I(q)$ , while a rough surface having  $2 < D_s \leq 3$  results in a slower decay of  $I(q)$ , with increasing  $q$  rather than  $q^{-4}$ . For all of the samples, we obtained a scaling of  $I(q) \propto q^{-3}$  at high- $q$  ( $> 0.3 \text{ nm}^{-1}$ ). This yields  $D_s \approx 3$ , which is characteristic of very rough interfaces. This is important evidence of the formation of highly porous structure

inside the particles. The high- $q$  peak located in  $1.5 < q/\text{nm}^{-1} < 2$  (the blue-colored region in **Fig. 3**) corresponds to the interlayer spacing of  $4.0 \pm 0.2 \text{ nm}$ . This is likely to be due to the reflection from the mesostructural periodicity observed in **Figs. 1** and **S2**.

To evaluate the electrocatalytic activity of MPNs, electrocatalytic oxidation of formic acid was tested and compared to commercially available Pd black (PB) and fine Pd nanoparticles (with 3 nm in diameter) (**Fig. S15**). **Fig. S15a** shows the cyclic voltammograms (CVs) in 0.5 M H<sub>2</sub>SO<sub>4</sub> containing 0.5 M HCOOH, showing a general behavior for formic acid oxidation on Pd electrode.<sup>[12]</sup> The presence of highly porous structure is very useful for acceleration of oxidation reaction. Our MPNs prepared under typical condition (1.0wt% F127) demonstrated the highest mass-specific activity of  $735.6 \text{ mA} \cdot \text{mg}^{-1} \text{ Pd}$ , which was 2.8 and 6.8 times higher than that of PB ( $259.5 \text{ mA} \cdot \text{mg}^{-1} \text{ Pd}$ ) and Pd nanoparticles ( $108.2 \text{ mA} \cdot \text{mg}^{-1} \text{ Pd}$ ). This mass activity of our MPNs is also higher than those of other state-of-art Pd-based, and even Pt-based nanomaterials reported previously, such as concave tetrahedral/trigonal bipyramidal Pd nanocrystals<sup>[13a]</sup>, MWCNTs supported Pd (Pd/MWCNTs)<sup>[13b]</sup>, and ultrathin single-crystal Pt nanowires<sup>[13c]</sup>.

Furthermore, we tested MPNs with different particle sizes, prepared with varied F127 concentration (0.00 wt%, 0.25 wt%, and 1.00 wt%). Their average particle sizes were 42 nm, 34 nm, and 28 nm, respectively. The smallest sized MPNs showed a remarkably large current density for electrocatalytic oxidation of formic acid, in comparison to the other larger-sized samples. The above results reveal that using small-sized MPNs allow reactants (guest molecules) to access all of the inner mesopores more easily without serious diffusion resistance. With the decrease of the particle sizes, the ECSAs calculated from CVs were increased from  $17.7 \text{ m}^2 \cdot \text{g}^{-1}$  (0.00 wt% F127) to  $48.6 \text{ m}^2 \cdot \text{g}^{-1}$  (0.25 wt% F127) and  $61.8 \text{ m}^2 \cdot \text{g}^{-1}$  (1.00 wt% F127). This maximum surface area was higher than those of Pd black ( $47.8 \text{ m}^2 \cdot \text{g}^{-1}$ ) and Pd nanoparticles ( $22.3 \text{ m}^2 \cdot \text{g}^{-1}$ ). Thus, the creation of mesoporous structure in small-sized MPNs can realize high surface area without its serious loss by ‘nanoparticle aggregations’ which have been often observed in electrode preparation using nanoparticles. Interestingly, even after normalization of the electrocatalytic activity by the surface area, the smallest size MPNs still exhibited very high specific activity ( $238.1 \text{ mA} \cdot \text{cm}^{-2}$ ) which was more than 2 times higher than those of PB and Pd nanoparticles (**Fig. S15b**). The periphery of MPNs exhibits curvature and highly roughened surfaces, which is generally the basis for the high catalytic activity in metal catalyst (**Fig. S6**).<sup>[14]</sup> Thus, it is clear that a significant increase of utilization efficiency of the Pd catalysts is achieved by introducing the mesoporous structures.

With further increasing the potential in the positive scan, the current densities were dropped due to the formation of Pd oxide, and the surface remained inactive until the reduction of Pd oxide surface took place. An important observation from the CVs is that the current densities for the negative and positive scans were nearly identical, and it was highly reproducible in consecutive scans, indicating a low tendency for poisoning of electrode surfaces due to adsorbed intermediates.<sup>[15]</sup> From the chronoamperometric plots (**Fig. S15c-d**), it was also confirmed that our small-sized MPNs showed the superior activity toward the formic acid oxidation. Even after 3000s chronoamperometric tests, our MPNs shows excellent stability compared to the other Pd samples (**Fig. S16**).

To conclude, we demonstrated a successful synthesis of

uniformly sized MPNs by utilizing both cationic surfactants and nonionic block copolymers with different functions; a structure-direct agent and a protective agent for controlled Pd deposition, independently. The average particle size could be controlled in a range from 25 nm to 42 nm without any influence on the mesostructural ordering. Metal-based mesoporous architectures allow high accessibility of guest molecules from the outside, realizing effective utilization of pores in nanosized particles. Our strategy could be applied to other metals and alloys. Further tuning of reaction conditions holds promise for achieving even more complex architectures, such as core-shell and yolk-shell structures. We strongly believe that our metal-based MNs can open a range of new application opportunities different from traditional silica- and carbon-based MNs.<sup>[2]</sup>

## Notes and references

<sup>a</sup> World Premier International (WPI) Research Center for Materials Nanoarchitectonics (MANA), National Institute for Materials Science (NIMS), 1-1 Namiki, Tsukuba, Ibaraki 305-0044 (Japan).

<sup>b</sup> E-mail: Yamauchi.Yusuke@nims.go.jp

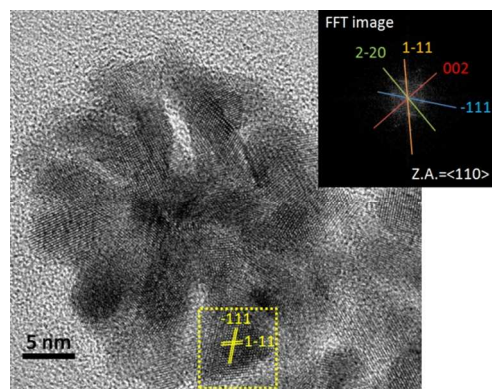
<sup>c</sup> Shinshu University, Tokida 3-15-1, Ueda, Nagano 386-8567 (Japan).

<sup>d</sup> Faculty of Science and Engineering, Waseda University, 3-4-1 Ohkubo, Shinjuku, Tokyo 169-8555 (Japan).

<sup>†</sup> Electronic Supplementary Information (ESI) available: Experimental procedure, characterization data of the deposited Pd samples and the used precursor solutions. See DOI: 10.1039/b000000x/

- (a) W. Li and D. Zhao, *Chem. Commun.* 2013, 49, 943; (b) C. T. Kresge and W. J. Roth, *Chem. Soc. Rev.* 2013, 42, 3663; (c) Y. Yamauchi, *J. Ceram. Soc. Jpn.* 2013, 121, 831; (d) K. C. W. Wu, X. Jiang, Y. Yamauchi, *J. Mater. Chem.* 2011, 21, 8934.
- (a) K. Ma, H. Sai and U. Wiesner, *J. Am. Chem. Soc.* 2012, 134, 13180; (b) Y. S. Lin, N. Abadeer, K. R. Hurley and C. L. Haynes, *J. Am. Chem. Soc.* 2011, 133, 20444; (c) T. Suteewong, H. Sai, R. Cohen, S. Wang, M. Bradbury, B. Baird, S. M. Gruner and U. Wiesner, *J. Am. Chem. Soc.* 2011, 133, 172; (d) T. W. Kim, P. W. Chung, I. I. Slowing, M. Tsunoda, E. S. Yeung and V. S. Y. Lin, *Nano Lett.* 2008, 8, 3724; (e) J. Liu, T. Yang, D. W. Wang, G. Q. (Max) Lu, D. Zhao and S. Z. Qiao, *Nature Commun.* 2013, 4, 2798; (f) J. Liu, S. Z. Qiao, H. Liu, J. Chen, A. Orpe, D. Zhao and G. Q. (Max) Lu, *Angew. Chem. Int. Ed.* 2011, 50, 5947; (g) L. J. Eun, N. Lee, T. Kim, J. Kim and T. Hyeon, *Acc. Chem. Res.*, 2011, 44, 893; (h) T. Suteewong, H. Sai, J. Lee, M. Bradbury, T. Hyeon, S. Gruner and U. Wiesner, *J. Mater. Chem.*, 2010, 20, 7807. (i) K. C. W. Wu and Y. Yamauchi, *J. Mater. Chem.* 2012, 22, 1251; (j) Y. D. Chiang, H. Y. Lian, S. Y. Leo, S. G. Wang, Y. Yamauchi and K. C. W. Wu, *J. Phys. Chem. C*, 2011, 115, 13158.
- (a) J. Lee, J. Kim and T. Hyeon, *T. Chem. Commun.* 2003, 1138; (b) J. Lee, S. Yoon, T. Hyeon, S. M. Oh and K. B. Kim, *Chem. Commun.* 1999, 2177; (c) H. Y. Lee, S. Ryu, H. Kang, Y. W. Jun and J. Cheon, *Chem. Commun.* 2006, 1325; (d) K. B. Lee, S. M. Lee and J. Cheon, *Adv. Mater.* 2001, 13, 517; (e) H. Kang, Y. W. Jun, J. I. Park, K. B. Lee, and J. Cheon, *Chem. Mater.* 2000, 12, 3530; (f) H. Wang, H. Y. Jeong, M. Imura, L. Wang, L. Radhakrishnan, N. Fujita, T. Castle, O. Terasaki and Y. Yamauchi, *J. Am. Chem. Soc.* 2011, 133, 14526; (g) H. J. Shin, R. Ryoo, Z. Liu and O. Terasaki, *J. Am. Chem. Soc.* 2001, 123, 12426.
- (a) C. Albayrak, G. Barim and Ö. Dag, *Chem. Eur. J.* 2013, 19, 15026; (b) C. Albayrak, A. M. Soyulu and Ö. Dag, *Langmuir* 2008, 24, 10592; (c) G. S. Attard, C. G. Göltner, J. M. Corker, S. Henke and R. H. Templer, *Angew. Chem. Int. Ed. Engl.* 1997, 36, 1315; (d) G. S. Attard, P. N. Bartlett, N. R. B. Coleman, J. M. Elliott, J. R. Owen and J. H. Wang, *Science* 1997, 278, 838-840.
- (a) X. Huang, Y. Li, Y. Chen, E. Zhou, Y. Xu, H. Zhou, X. Duan and Y. Huang, *Angew. Chem. Int. Ed.* 2013, 52, 2520. (b) F. Wang, C. Li, L. D. Sun, C. H. Xu, J. Wang, J. C. Yu and C. H. Yan, *Angew. Chem. Int. Ed.* 2012, 51, 4872. (c) S. Yang, C. Shen, X. Lu, H. Tong, J. Zhu, X. Zhang and H. J. Gao, *Electrochimica Acta* 2012, 62, 242.
- (a) S. Areva, C. Boissière, D. Grosso, T. Asakawa, C. Sanchez and M. Lindén, *Chem. Commun.* 2004, 1630; (b) K. Suzuki, K. Ikari and H. Imai, *J. Am. Chem. Soc.*, 2004, 126, 462; (c) H. Mori, M. Uota, D. Fujikawa, T. Yoshimura, T. Kuwhara, G. Sakai and T. Kijima, *Microporous Mesoporous Mater.* 2006, 91, 172.
- (a) A. L. Wang, H. Xu, L. X. Feng, L. X. Ding, Y. X. Tong and G. R. Li, *J. Am. Chem. Soc.* 2013, 135, 10703; (b) P. F. Siril, L. Ramos, P. Beaunier, P. Archirel, A. Etcheberry and H. Remita, *Chem. Mater.* 2009, 21, 5170.
- (a) K. Torigoe and K. Esumi, *Langmuir* 1992, 8, 59; (b) C.-W. Yang, K. Chanda, P.-H. Lin, Y.-N. Wang, C.-W. Liao and M. H. Huang, *J. Am. Chem. Soc.* 2011, 133, 19993; (c) B. Veisz and Z. Kiráky, *Langmuir* 2003, 19, 4817; (d) G. Berhault, M. Bausach, L. Bisson, L. Becerra, C. Thomazeau and D. Uzio, *J. Phys. Chem. C* 2007, 111, 5915.
- I. Sokolov, H. Yang, G. A. Ozin and G. S. Henderson, *Adv. Mater.* 1997, 9, 917.
- (a) M. Wang, Z. Sun, Q. Yue, J. Yang, X. Wang, Y. Deng, C. Yu and D. Zhao, *J. Am. Chem. Soc.* 2014, 136, 1884; (b) Z. Zhang, Y. Han, F.-S. Xiao, S. Qiu, L. Zhu, R. Wang, Y. Yu, Z. Zhang, B. Zou, Y. Wang, H. Sun, D. Zhao and Y. Wei, *J. Am. Chem. Soc.* 2001, 123, 5014.
- Teixeira, J. *J. Appl. Cryst.* 1988, 21, 781.
- (a) V. Celorrio, M. G. Montes de Oca, D. Plana, R. Moliner, M. J. Lázaro and D. J. Fermin, *J. Phys. Chem. C* 2012, 116, 6275; (b) W. P. Zhou, A. Lewera, R. Larsen, R. I. Masel, P. S. Bagus and A. Wieckowski, *J. Phys. Chem. B* 2006, 110, 13393.
- (a) X. Huang, S. Tang, H. Zhang, Z. Zhou and N. Zheng, *J. Am. Chem. Soc.* 2009, 131, 13916; (b) A. B. A. Nassr, A. Quetschke, E. Koslowski and M. Bron, *Electrochim. Acta* 2013, 202; (c) B. Y. Xia, H. B. Wu, N. Yan, X. W. (David) Lou and X. Wang, *J. Am. Chem. Soc.* 2013, 135, 9480.
- (a) T. Fujita, T. Tokunaga, L. Zhang, D. Li, L. Chen, S. Arai, Y. Yamamoto, A. Hirata, N. Tanaka, Y. Ding and M. Chen, *Nano Lett.* 2014, 14, 1172; (b) H. Wang, L. Wang, T. Sato, Y. Sakamoto, S. Tominaka, K. Miyasaka, N. Miyamoto, Y. Nemoto, O. Terasaki and Y. Yamauchi, *Chem. Mater.* 2012, 24, 1591.
- M. Baldauf and D. M. Kolb, *J. Phys. Chem.* 1996, 100, 11375.

A table of contents



<sup>5</sup> We report a solution phase synthesis of monodispersed mesoporous Pd nanoparticles (MPNs) with narrow particle size distributions.